**Proceedings of ASME 2013 International Design Engineering Technical Conferences &
Computers and Information in Engineering Conference
IDETC/CIE 2013
August 4-7, 2013, Portland, Oregon, USA**

DETC2013-12790

INCREMENTAL INSPECTION FOR MICROROBOTIC QUALITY ASSURANCE

David L. Christensen
Elliot W. Hawkes
Biomimetics and Dexterous Manipulation Laboratory
Department of Mechanical Engineering
Stanford University
Stanford, California 94305-2232
Email: davidc10@stanford.edu

Annjoe Wong-Foy
Ronald E. Pelrine
Robotics Program
Engineering Systems Group
SRI International
Menlo Park, California 94025-3493
Email: ronald.pelrine@sri.com

Mark R. Cutkosky
Biomimetics and Dexterous Manipulation Laboratory
Department of Mechanical Engineering
Stanford University
Stanford, California 94305-2232
Email: cutkosky@stanford.edu

ABSTRACT

This paper addresses inspection techniques that can be performed by microrobots used for fabricating three dimensional structures. In contrast to most commercial rapid prototyping processes, the parallelism afforded by microrobot teams allows incremental inspection of structures during assembly. In the present case, this approach is applied to parts fabricated from carbon fiber struts bonded with UV-cured epoxy. Preliminary tests involving thermal and vibrational inspection methods are described and compared with the results of FEA models of the joints. Vibrational inspection performed by microrobots and recorded using a directional microphone, characterizes bond joint natural frequency with good resolution (an average measurement standard deviation of 5Hz over a range of 650-1215 Hz). These effective stiffness measurements are correlated with ultimate bond strength as well. The measurements are sufficient to distinguish between joints that do or do not have desired amounts of adhesive.

KEYWORDS: MICROROBOTS, MANUFACTURING, QUALITY CONTROL, ASSEMBLY, INSPECTION

INTRODUCTION

Advances in technology are leading to the possibility that swarms of microrobots could work together to fabricate three-dimensional structures, drawing inspiration from the ways in which wasps or termites build a nest. Among the potential advantages of this approach is massive parallelism: the ability to perform many discrete operations simultaneously for a potentially much greater throughput than would be possible using other free-form fabrication techniques like 3D printing with a few deposition heads. Teams of miniature robots can also work with heterogeneous mix of materials including solids (plastics, metals, wood) and even manufactured electronic components, optics or high quality bearings. Early examples of parallel microrobotic systems include [1–10]. In related work, several investigations have explored sensing [11–14], and fabrication and/or inspection of parts [4, 15–18].

Another potential advantage of microrobotic swarms is the ability to perform certain inspection and quality insurance tests incrementally and *in-situ*, as a part or a structure is created. This is something that is regularly done when building large civil engineering structures, for example by testing each new pour of concrete or inspecting the welds on a structure as it is fabricated. However, it is generally not possible when manufacturing small components, whether by conventional means or modern rapid-prototyping methods. Instead, one must wait until the part is finished to subject it to inspection and testing. There is even the possibility that a hidden internal defect will not be found, leading ultimately to a failure in service.

With a team of microrobots building a structure it is possible to allocate some of them to testing newly fabricated sections. It is even possible to consider an "undo" function such that if a defect is found, the offending part of the structure is cut away and rebuilt without having to scrap the entire part.

The concept of incremental inspection with microrobots is the motivation behind the work presented in this paper. The specific context is a microrobotic platform developed at SRI [9] consisting of small (presently $3\times3\times0.5$ mm) magnetic devices that are propelled across a circuit board (Figs. 1, 2). Early demonstrations of this platform [10] have focused on assembling truss structures of carbon fiber struts bonded with UV-cured epoxy resin to create three dimensional space frames of carbon fiber elements (Fig. 2 (left) shows one such microrobot-constructed truss under load). While the goal of the manufacturing process is to minimize bonding errors and variability, a good process also includes quality control as feedback for the errors that will inevitably occur. Therefore, the focus of the work reported here is to examine two different inspection methods that could be applied to check

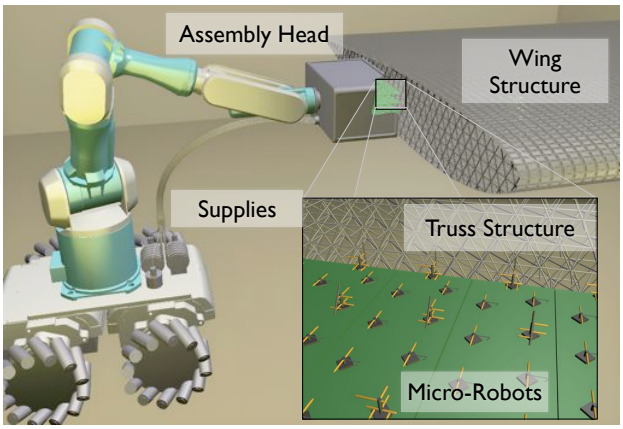

FIGURE 1. CONCEPTUAL RENDERING OF THE SRI MICROROBOTIC MANUFACTURING PROCESS.

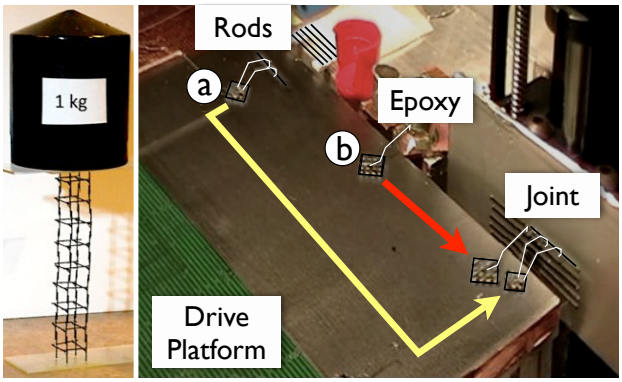

FIGURE 2. *LEFT:* AN EXAMPLE OF A TRUSS STRUCTURE BUILT BY MICROROBOTS. *RIGHT:* PHOTOGRAPH OF TWO MICROROBOTS WORKING AS A TEAM TO BUILD A TRUSS ELEMENT. ONE PICKS AND PLACES CARBON FIBER RODS (A) WHILE THE OTHER DEPOSITS EPOXY (B). OUTLINES OF ROBOTS AND END EFFECTORS TRACED FOR VISUAL CLARITY.

the quality of joints, as these are the main contributors to discrepancies between the actual versus expected stiffness and strength. The approach described here is potentially applicable to other microrobotic manufacturing systems that involve the assembly of bonded structures.

The following sections first briefly describe the carbon rod assembly process and the options for inspection. Next, two candidate inspection methods, one thermal and one involving vibration analysis, are introduced and results are provided for test assemblies of carbon fiber struts. It is shown that while the thermal approach can sense the presence of a bond before it is set and may be useful for processes that are inherently heat-intensive (e.g., thermoplastic forming or heat curing), the vibration analysis provides a clearer signal that is directly related to the coverage and quality of an epoxy joint. These factors are, in turn, related to the stiffness of the structure. Finally, tests confirm that joint stiffness is directly correlated to ultimate strength allowing microrobotic prediction of both stiffness and strength. The paper concludes with a discussion of future work, including integration of the test methods into robotic swarm manufacturing for true incremental *in-situ* bond inspection of large parts.

1 Assembly Process and Sensing Objectives

The SRI microrobotic system consists of millimeter scale magnets formed into arrays. Magnetic field patterns are generated on the surface of a platform by flowing current through traces, and the magnet arrays align themselves to these generated magnetic fields. As the amount and direction of current is varied through the layers of traces, the magnetic fields move and the robots follow them like permanent magnets in a stepper motor, forming a two dimensional surface motor [19].

The manufacturing goal is to create a structure consisting of many small carbon fiber rods joined together into a truss. The rod material is prefabricated in bulk, and a dispenser cuts millimeter to centimeter scale segments, dispensing them individually to the robots as needed. A rod pick-and-place robot (Fig. 2(right, a)) has a specialized end effector with hydrophilic zones that use water surface tension to grab and align rods. While a rod is being picked, a second robot (Fig. 2(right, b)) with another specialized end effector picks up a droplet of epoxy from a dispenser and places it on the intended joint location. The first robot then places the rod into the epoxy droplet at the joint location and a UV light source (LED) is energized to cure the epoxy in place. As the robot retreats, the water surface tension is easily broken leaving the completed truss element with the robots free to perform another cycle. This process (visible in action in an online video[1]) would be performed in parallel with many micro robot teams to complete a large structure quickly.

In this application, measurements of both the strength of the truss joining bonds (the strength limiting feature) and the bond stiffness are useful as quality control and predicted performance metrics. Further, such metrics can act as a process check since the robots are performing without direct feedback. Equations (1-3) introduce some physical properties of a joint that depend on material properties and geometry (Fig. 3 (top)). Equation (1) shows that while the shear strength should scale as radius squared, an imperfect truss joint will be loaded with moment as well which is limited by Eqn. (2).

$$F_{max} = \pi r^2 \sigma_{max} \quad (1) \qquad T_{max} = \frac{\pi r^3}{2\tau_{max}} \quad (2)$$

where r is the bond radius and σ_{max} and τ_{max} are respectively the tensile and shear yield strength of the bond material. A possible third power dependency on radius indicates that an ideal measurement to predict strength should be sensitive to adhesive at the outer diameter of the bond.

If the measure of interest is stiffness, the dependence of the torsional stiffness, K_t, on radius is

$$K_t = G\frac{J_t}{h} \text{ where } J_t = \frac{\pi r^4}{2} \quad (3)$$

G is the shear modulus of the bonding material and h is the bond height between rods.

The small size of the individual robots, their lack of onboard feedback and the intended parallelism of the manufacturing task lead to a unique set of constraints when choosing a sensing mode to convey strength. While a direct stress-strain test would be an ideal way to measure stiffness, due to their small size, the robots are unable to provide

[1] http://www.scientificamerican.com/article.cfm?id=sri-magnetic-microbot-construction

enough force to make this practical. While a measurement of heat transfer across a joint could indicate a contact area of the glue, the robots' lack of onboard feedback could give misalignment errors resulting in bad thermal conductivity measures. Finally, while image processing would be convenient for obtaining the geometry of the bond in a non-contact manner, the image sensing and processing would scale poorly with the intended parallelism of the process. Ideally the inspection process should require little force, be relatively insensitive to robot alignment, and scale potentially to hundreds or thousands of inspection sites.

For this work, two promising sensing modes were chosen as preliminary indicators for strength of a simple "L" joint: thermal resistance of the joint, and resonant frequency of the free end of the "L."

2 Thermal Inspection

2.1 Methods

For the case of thermal inspection, the bond is treated as a thermal resistance that depends on the geometry of the glue. There are two simple ways to interrogate the system. The first involves inducing heat flux through the joint and examining the temperatures across it. The second examines the time constant to equilibrate a thermal charge across the joint (this involves both thermal resistances and heat capacities). A thermal schematic is shown in Fig. 3 which represents a cross section of a joint between two orthogonal carbon fiber struts bonded with epoxy. The joint can be viewed as a set of thermal resistances in parallel according to Eqn. (4). The heat will take the shortest path through the epoxy (seen in the center); so the center area will dominate the overall thermal resistance. While this will result in good sensitivity to glue in the center, the joint stiffness and strength are dominated by the glue at the extents (Eqns. (2), (3)). Therefore the measure will only be useful in cases with a good ratio of signal to noise.

This method can be considered a thermometric measurement and is related to inspection methods previously used for aerospace composites [20] albeit on a much smaller scale.

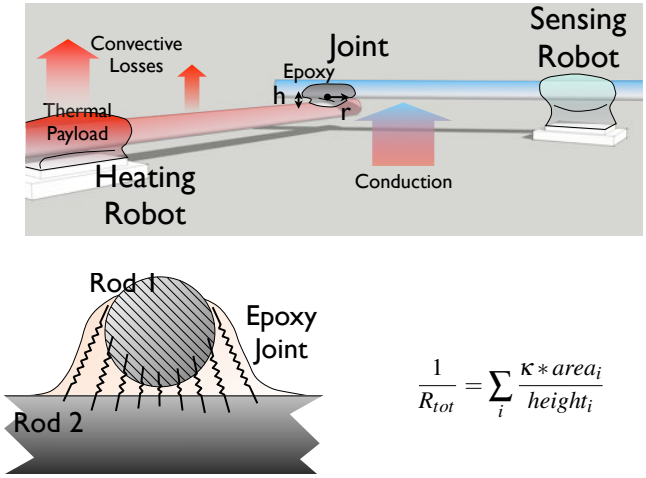

$$\frac{1}{R_{tot}} = \sum_i \frac{\kappa * area_i}{height_i} \qquad (4)$$

FIGURE 3. THERMAL DIAGRAM AND THERMAL RESISTANCES APPROXIMATING A JOINT.

A simple thermal FEA model (Table 1) was constructed using COMSOL to solve the system of thermal resistances. The model is run to examine peak temperature differential due to fixed heat flux across the joint while varying bond size as well as the ratio of thermal conductivity between the rods and the glue. Results were checked for convergence by re-meshing on three progressively smaller cell sizes to ensure consistency. Tests were run sweeping the bond geometry size from 0.1 to 2 rod diameters. Temperatures upstream and downstream of the joint were recorded.

TABLE 1. VALUES USED FOR THERMAL STEADY STATE FEA MODEL.

Property	Value
"physics controlled" cells	20,000 3D Tetrahedral
rod [21], bond[2] thermal conductivity	1.4 W/mK, 0.2 W/mK
rod diameters, lengths	1 mm, 10 mm
rod 1, 2 end boundaries	100 W/m^2 source, 20°C sink
all other boundaries	perfect insulation

An enlarged physical model was constructed to gain intuition and verify the findings of the FEA model. The joints (Fig. 4 (a), (b)) consisting of unidirectional carbon fiber rods, 6 mm diameter by 50 mm long, were large enough for imaging with a Raytheon L-3 Thermal-Eye 500D infrared camera with a temperature resolution of 0.1°C. Portions of the setup were locally heated with a heat gun while suspended in air.

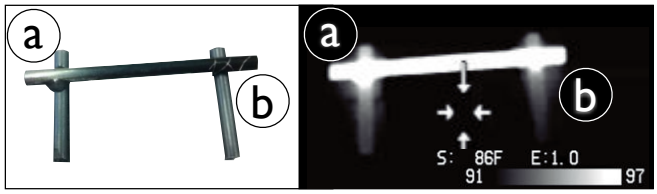

FIGURE 4. *LEFT:* PHOTOGRAPH OF ENLARGED PHYSICAL MODEL WITH BONDED JOINT (A) AND UNBONDED JOINT HELD IN PLACE WITH FINE WIRE (B). *RIGHT:* CORRESPONDING IR IMAGES SHOWING THE DIFFERENCE IN TEMPERATURE AT EACH JOINT DURING HEATING. IMAGE SHOWS 0.3°C LOWER DIFFERENTIAL IN THE BONDED CASE.

Finally, to test the feasibility of thermal inspection at the intended scale, a simple jig (Fig. 5) was built to hold bonded or unbonded rods, thermocouples (Type K) for temperature measurement, and a small reservoir to contain a thermal payload. Care was taken to minimize thermal losses to the jig. For testing, 0.95 mm diameter by 25 mm long unidirectional carbon fiber rods were inserted into the jig. A very small clamping force was provided by the spring preload from the thermocouples, ensuring thermal contact between the temperature sensors and the rods, as well as between the rods themselves. Tests were performed on the rod setup before and after applying Devcon 5 Minute Fast Drying Epoxy (with thermal conductivity similar to UV cured epoxy used with

[2] http://www.unicomposite.com/products/carbon\%20fiber\%20tube.htm

the robots) to the joint. Thermocouple temperatures were recorded over several minutes at 2 Hz by two handheld meters (Supco EM90) with an estimated resolution of 0.1°C.

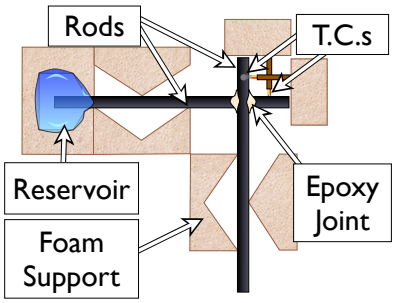

FIGURE 5. SCHEMATIC OF EXPERIMENTAL SETUP FOR TESTING THERMAL RESISTANCE ACROSS JOINT.

Boiling water was chosen as the heat source for its high specific heat; 4 to 6 droplets (totaling 0.25 mL +/-0.05 mL) were dispensed into the reservoir using a manual dropper. While the water bath itself was maintained at 100°C, the temperature dropped substantially (approximately 30°C down to 70°C +/-15°C) during dispensing due to convective and conductive losses to the environment and setup. Using a differential temperature measurement helps with this temperature variability, but it remains a source of error in the experiment.

Measurements of interest included a comparison of the decay rates of the differential temperature across the joint and the maximum differential observed in the course of measurement. These values were examined before and after a typical amount of glue was added to a joint.

2.2 Thermal Results

As seen in Fig. 6 (left) the thermal decay rates do not have a strong correlation with bonding condition (they may be dominated by convection losses to ambient instead of conduction between the rods). However, the peak temperature difference, averaged over many samples (Fig. 6 (right)), does show a statistically significant difference between unbonded and bonded cases.

Measuring before and after applying glue showed a positive change in conductivity for every joint, and 87.5% of the bonded joint results were higher than the highest unbonded result.

Variability in the amount of heat added is one clear source of error that is mitigated with the differential measurement used, but this will be a challenge for a microrobotic platform. A high surface area to volume ratio gives small water droplets relatively fast time constants, and makes useful heat retention difficult. This could be mitigated by using a direct heat source such as a laser or resistance heating leads. Another option is a phase change material such as wax to contain the thermal payload instead of water.

While the results show statistical significance for sensing the presence of glue in a joint, testing did not show a strong dependence on the *amount* of glue present. For the sake of understanding the system better, a series of tests were performed on the FEA model (the ideal noiseless system) previously mentioned. As seen in Fig. 7, this thermal system is quite sensitive to having glue at the center of the bond where the distances between the carbon rods are very small and the overall joint area

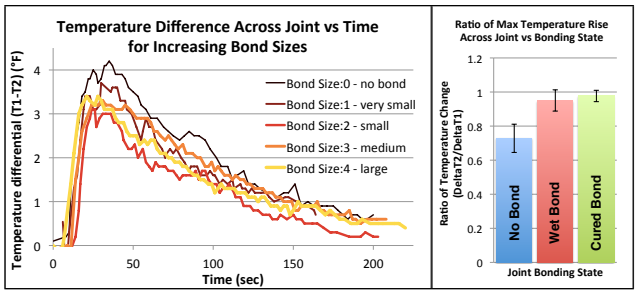

FIGURE 6. *LEFT:* TYPICAL PROFILES OF TEMPERATURE ACROSS JOINT VS TIME. *RIGHT:* RATIO OF PEAK TEMPERATURE RISE UPSTREAM AND DOWNSTREAM OF THE JOINT VS BONDING STATE. LOWER VALUES REPRESENT HIGHER DIFFERENTIALS.

is small, but is insensitive to adding glue at the periphery of a joint. Furthermore the shape of this dependency remains constant and simply scales as the relative thermal conductivity between the carbon fiber rod and the epoxy changes.

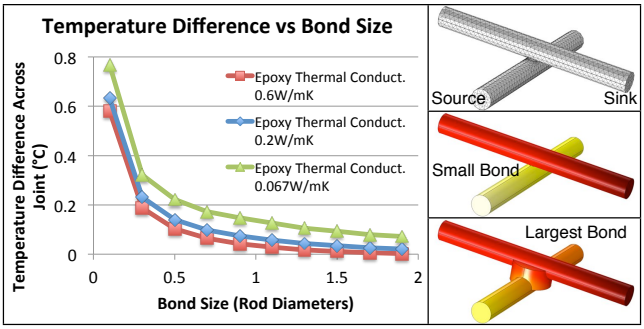

FIGURE 7. *LEFT:* RESULTS FROM FEA MODEL SHOWING TEMPERATURE DIFFERENCE ACROSS A JOINT FOR DIFFERENT GLUE CONDUCTIVITIES AND JOINT AREAS. *RIGHT:* A SAMPLE MESH AND TWO SAMPLE GEOMETRIES.

These results provide some intuition about the system; the unbonded cases had a higher variance because of the relative importance of the details at the center point of contact. The low sensitivity for bond sizes larger than 0.2 rod diameters explains the measured lack of dependence on glue amount. The perfect insulation and perfect source assumptions that produce an asymptote at zero bond area would not be expected with rod contact and convection. We also note a lack of a thermal gradient on the "dead ends" beyond the joint. This makes these regions good places to measure with robots since the measurement is insensitive to location. This effect was verified in our enlarged physical model as well.

The model predicts that in order to get useful information on the size of a joint larger than about half a rod diameter, the robots would need a very accurate and high resolution measurement of temperature – better than about 0.02°C with very little drift or error. While amply miniaturized thermocouples are readily available commercially (down to about 0.050 mm diameter) there are large concerns with noise from

unshielded wire near the drive board . Running the measurement at a known frequency (e.g., at 10 Hz) would help but is difficult with robots providing the thermal payload. More power will help as well, however microrobot integration will impose limits on both these options. It is also worth noting that the time between measurements for everything to cool to ambient was substantial (on the order of minutes), making sequential measurements very time consuming.

These challenges are not insurmountable, but will require considerable effort to overcome. The measurement would be more attractive for use in cases where construction is already a heat activated process, removing the need for additional heating equipment. The method also suits cases in which one is primarily concerned about sensing a "kissing joint" (very small bond) and does not care about relative sizes of larger joints. Finally, the method is most useful where one would like to sense the presence of glue in the joint before it is cured and thus can still be fixed easily.

3 Vibrational Inspection

3.1 Methods

We consider the carbon fiber strut to be a cantilever beam attached with a lumped torsion spring at its base. In the limiting case that the glued joint is very stiff, the first natural frequency of the beam approaches that of a cantilever with a clamped base [22]

$$f_{n1} = \frac{1.875^2}{2\pi}\sqrt{\frac{EI}{\rho L^4}} \tag{5}$$

where $\rho = m/L$ is the mass per unit length, E is the Young's modulus of the material and I is the moment of inertia of the beam cross section. Conversely, if the glue joint is quite small, it approaches the case of a rigid rod with a torsion spring at its base

$$f_n = \frac{1}{2\pi}\sqrt{\frac{3K_t}{mL^2}} \tag{6}$$

where K_t is given by Eqn. 3. Between the limiting cases of Eqs. 5 and 6, the resonant frequency shows good sensitivity to bond size, as seen in Fig. 8.

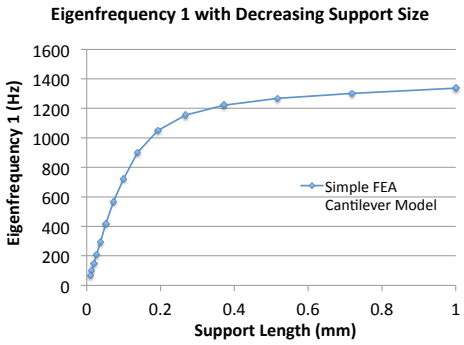

FIGURE 8. RESULTS FROM A SIMPLE FEA CANTILEVER MODEL WITH A PROGRESSIVELY REDUCED SUPPORT SIZE SHOWING THE CHANGE OF THE FIRST EIGENFREQUENCY AS JOINT SIZE APPROACHES ZERO.

TABLE 2. VALUES USED FOR VIBRATION FEA MODEL.

Property	Value
"physics controlled" cells	2E4 to 4E4 3D tetrahedral
Young's modulus of rod[3], bond[4]	120E9 Pa, 1.2E9 Pa
ν (rod, bond), ρ(rod, bond)	(0.3, 0.4), (1600, 1360)kg/m^3
rod1, rod2 (diameter, length)	(0.72, 4.7), (0.72, 25)mm
rod 1 end boundary, all others	fixed, free

Measurements of natural frequencies have been used to characterize engineering structures and materials before ([23], [24] among many others) and have provided good data with simple and low cost apparatus, thanks in part to the pseudo-digital nature of frequency-as-measurement signals.

To examine this vibrational inspection concept, a simple model was built (again in COMSOL) to perform an Eigenmode/Eigenfrequency study as the bond size was changed (Fig. 10). The geometry studied was a simple "L" shaped joint with one end fixed and had a fixed constraint a quarter of the way down the length of the supporting shaft. Results were again verified for convergence by running with 3 smaller mesh sizes and verifying consistency.

To test the vibrational inspection concept, a joint bonded with cyanoacrylate (CA) adhesive and cured with accelerator, was mounted in a clamp (with 0.68 mm diameter and 25 mm long rods). The rod end was plucked manually (Fig. 9(bottom, a)) exciting its resonant frequencies. The lowest in plane mode was targeted, though others were occasionally evident as well.

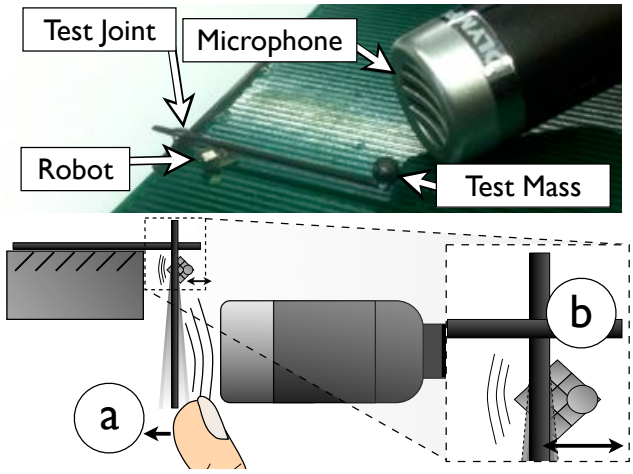

FIGURE 9. *TOP:* MICROROBOT, JOINT, AND MICROPHONE USED FOR INSPECTION. *BOTTOM:* SCHEMATIC OF SETUP FOR MANUALLY PLUCKED INSPECTION (A) AND MICROROBOT DRIVEN INSPECTION (B).

[3] http://www.acpsales.com/pds/CLs.pdf

[4] http://www.matweb.com/search/DataSheet.aspx?MatGUID=d0d7dbec7666421caf8aa08724b634c5

The sound of the ringing was recorded by a unidirectional microphone (Olympus ME52) placed 0.5 cm away, and hooked up to an audio card (Creative XPod) digitizing and recording the signal into an audio sampling program (Audacity). Since the bonded carbon rod joints have a high quality factor (on the order of 100), they produce long ringing signals that can be recorded and analyzed for spectral content. Data were recorded at 44 KHz. The quality factor of the rods and the sensitivity of the microphone allowed 2048 points for the spectral analysis which gives a resolution of 21.5 Hz/bin. A cubic fit is performed using the closest four points to the peak to find the interpolated maximum.

To test for the effect of glue with other variables constant, we initially bonded with the smallest amount of glue that could feasibly withstand testing, recorded an image of the joint under a microscope, tested, then added more glue to the joint and repeated (Fig. 13 (bottom) shows joint sizes). All tests were performed without removing the joint from the clamp to keep the boundary conditions consistent.

Obtaining good measurements for the "size" of the glue bond joint proved difficult and is the part of the measure with the largest uncertainty. To obtain useful data, we used two optical measures from the bond pictures: maximum distance between extents of the bond, and the radius of the largest circle that could be fit within its center area including the corner fillets (Fig. 13(bottom center)). These manual measurements are less than ideal, but if we assume the shape of all the bonds to be constant (in aspect ratios, not size) then the two measures should be correlated. We use a best fit line for the entire data set to find the ratio of the two measures (established from the shape) and then use the point of least distance from that line as the measured value for joint size.

Using the joint size and shape data, the previously discussed FEA model was modified to match the geometries of each of the progressively tested joints for comparison with the physical results. Figure 10 shows example joints comparing microscope images and corresponding model geometries used.

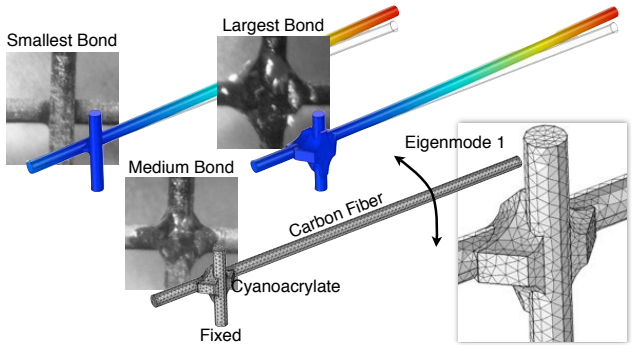

FIGURE 10. SAMPLE JOINT PICTURES AND CORRESPONDING FEA MODEL GEOMETRIES. BOTTOM FEA MODEL SHOWS A SAMPLE MESHING, WHILE UPPER TWO SHOW CALCULATED EIGENMODE SHAPES.

To perform a similar measurement using microrobots, structural modes are excited by repeatedly impacting the test joint with the 0.04 g microrobot (Fig. 9). The impacts are repeated at a frequency much lower than the structural mode of interest (about 60 Hz versus 600 Hz) and the resulting sound is recorded with the same setup previously discussed. The high quality factor of the carbon fiber structures again gives a spectral peak corresponding to its primary structural eigenfrequency. The quasi-continuous nature of this measurement compared to the discrete plucked tests allowed for much larger audio samples to be gathered: about 2 seconds worth allowing for 16384 points and a much finer spectral resolution of 1.3 Hz.

The same battery of physical tests is performed with this setup as with the plucked data, adding CA in stages to form a progressively larger joint, recording sound data and optical microscope images for both joint size, and measuring the resonant frequency. However the delicate microrobot measurement allowed several measured bonds small enough to be completely obscured by the rods themselves. Consequently, the approximate volume of deposited glue is used as a measure of joint size rather than optical measurement. This approximation is not ideal but adequate for examining the figures of interest: span and variance of the frequency measurement.

To characterize the performance of both the plucked and robot excited measurements, we define the resolution between two consecutive joint size tests as the frequency span divided by the average standard deviation of the measurements for those two tested sizes. By summing these resolutions between joint size tests over the entire tested range, a measure of the number of size resolution points of a typical joint is obtained Eqn. (7).

$$ResolvedLevels = \sum_{i=1}^{bins-1} \frac{(f_{n(i)} - f_{n(i+1)})}{(\sigma_{n(i)} + \sigma_{n(i+1)})/2} \tag{7}$$

Finally to demonstrate the relationship between measurements of natural frequencies and ultimate strength, another joint-size study is performed with each joint progressively loaded until failure. A jig was constructed for making joints with geometries repeatable to better than 0.5 mm, and the same rods reused for every test with careful cleaning, light sanding and an isopropyl alcohol wash before bonding. A variety of joint sizes were formed (again using CA and activator), without a fixed progression of size but with a target range of natural frequencies. Every bond was photographed under microscope and tested for natural frequency with microrobots by the method previously discussed.

A fixture holds the base of a joint pointed downwards. Spectra threads (100 pound test) looped and tied around the free rod apply load to the joint (Fig. 11). Since truss structures are the eventual manufacturing goal, the testing loads are applied close to the joint to keep testing loads dominantly in shear (as would be true for a well designed truss). Water serves as the testing load and is added (over the course of a few minutes per test) to a reservoir hanging from the threads. When the joint is broken, the water flow is stopped, and the load at failure is weighed with an electronic scale accurate to one gram. The time to shutoff the flow of water in response to the completion of the test gives a measurement uncertainty of 10 grams, however variability in the bonding conditions and process dominate the uncertainty in the experiment.

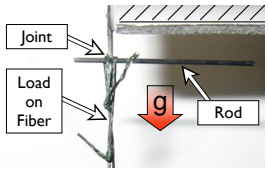

FIGURE 11. SETUP FOR DETERMINING THE ULTIMATE STRENGTH OF A BOND.

3.2 Vibration Results

The manually plucked excitations provided good data compared to thermal results. Fig. 12 shows a sample ringdown curve and resulting spectrum performed in Audacity (Hann window, 4096 points). The main resonant peak was always the largest peak above 150 Hz, and was well above the noise floor in this region. When measuring only the ring-down phase (cropping out the excitation), repeatability across multiple plucks was ± 3 Hz for all sets of measurements, or about 0.2% of the natural frequency, although there is a frequency dependence on amplitude that caused more error (0.5%) in a few outliers.

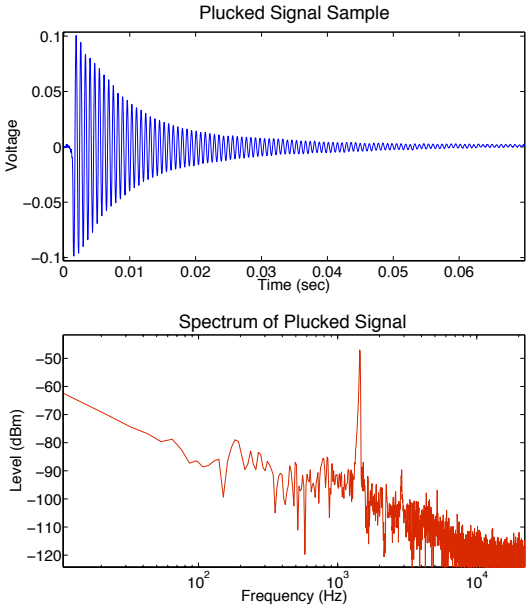

FIGURE 12. SAMPLE PLUCKED RINGING WAVEFORM AND CORRESPONDING SPECTRUM.

The results from the plucking tests with increasing joint sizes are seen in Fig. 13. Note that the error bars for the x-axis are the dominant error, with the y-axis error being indiscernible. The x-axis error bars represent the x-axis variability depending on the definition of size, either based on the diameter of the largest circle that fits within the bond, or the maximum extent that the bond covered. The trend between natural frequency and size is clearly discernible and in broad agreement with the FEA model results from the measured joint geometries. The average standard deviation of the natural frequency measurements is 1.5 Hz (with 8 measurements for each joint size). Using Eqn. (7), a spread of measured frequencies ranging from 1188 Hz to 1446 Hz results in 170 discernible one-sigma levels of stiffness (and therefore bond size) for this range of typical joint sizes. Recall that the minimum joint size is limited by the smallest joint that could survive plucking.

As seen in Fig. 14, the robot-excited test unsurprisingly yielded different results in the time domain. The data are composed of many low-energy, discrete strikes, and are visibly less clear. Upon careful inspection, however, Fig. 14 (top)) shows similar ring-down patterns albeit with much more noise, probably due to the excitation of many more

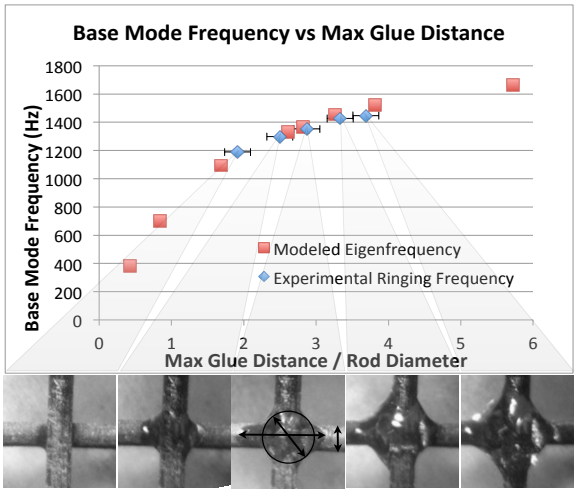

FIGURE 13. *TOP:* EXPERIMENTAL PLUCKED RINGING FREQUENCY AND MODELED EIGENFREQUENCY RESULTS FOR A JOINT WITH INCREASING BOND SIZE. Y-AXIS ERROR BARS ARE NOT VISIBLE ON THIS SCALE WITH A STANDARD DEVIATION OF LESS THAN 2 HZ. *BOTTOM:* MICROSCOPE PICTURES OF JOINTS, INCLUDING DIMENSIONS THAT DEFINE BOND SIZE.

modes. Despite the lower amplitudes and noisier signals, more data can be quickly obtained with this method, allowing the measurement to produce resolvable signals. The spectrum still shows a reasonably sharp peak corresponding to the first natural frequency of the joint. The higher frequency noise visible in the spectrum is believed to be a combination of at least one real resonant mode and sounds made as the robot rebounded from the collision, some of which has been eliminated with a redesigned striking-mass to prevent inducing moments during striking. In work subsequent to these tests, better lateral position control of the robots has been implemented, which should reduce the variance in the natural frequencies.

A sweep of bond sizes performed with robots yielded similar results to the plucked data, as seen in Fig. 15. The average measurement standard deviation was larger (4.8 Hz), but the lower forces involved allowed for measurement of joints that were much smaller without breaking. Again using Eqn. (7) the measured range of 650 Hz to 1215 Hz results in 107 one-sigma natural frequency levels (and again therefore joint sizes as well) over the tested range. This is a high enough resolution to not only check that the joint was bonded but to predict the overall stiffness and strength of a truss element as well. Likely estimates of stiffness will be more limited by other factors (such as variations in rod geometry, stiffness and density) than the accuracy of this natural frequency measurement.

As seen at the bottom of Fig. 15, the first two joint sizes measured (which incidentally yielded 13 resolved size levels between them) are too small to see in the microscope because they are completely obscured by the rods. While this represents a useful measurement capability, it presented a problem for the joint size data (x data) previously measured by optical inspection. As a replacement, the cube root of the total volume of glue applied to the joint in droplets ($0.05\text{mm}^3 \pm 0.02\text{mm}^3$) normalized by the single droplet used for the first joint was used instead. This results in possibly large errors for the x-axis. The test was sufficient to explore the range and resolution of possible micro robot measurements of representative joint geometries and stiffnesses, and the cube

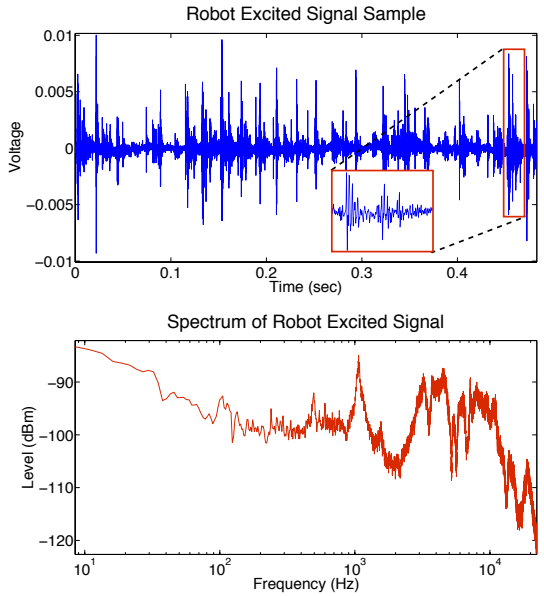

FIGURE 14. *TOP:* SAMPLE MICROROBOT EXCITED WAVEFORM. *BOTTOM:* CORRESPONDING SPECTRUM.

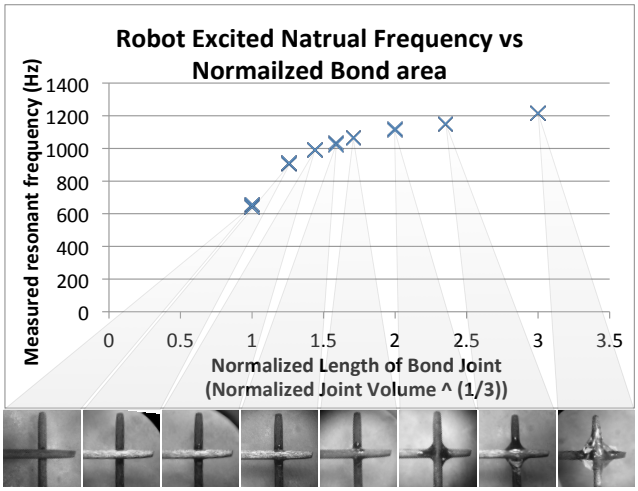

FIGURE 15. EXPERIMENTAL RESONANT FREQUENCY RESULTS FOR A JOINT OF INCREASING SIZE MEASURED BY ROBOT EXCITATION.

root of volume should make this curve roughly comparable in shape to the previous length scales in the plucked data.

The microrobot measured natural frequency compared to joint load failure tests can be seen in Fig. 16. The x-axis is chosen as natural frequency squared so that it would scale linearly with stiffness, effectively making this a comparison of bond stiffness versus strength. While the complicated geometry involved in the space at the intersection of the rods, and the geometric inability to load in pure shear, and the asymptote as the stiffness of the joint approaches the stiffness of the carbon

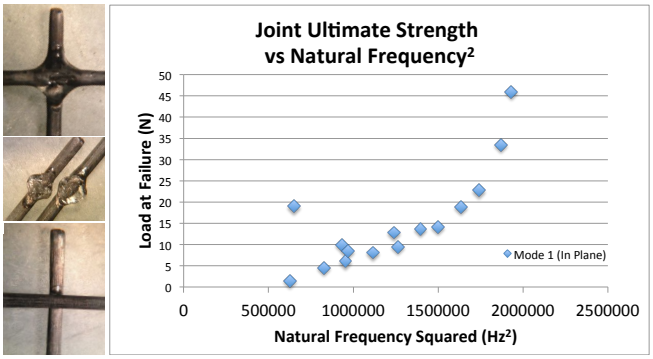

FIGURE 16. BOND STRENGTH AT FAILURE VS MICROROBOT MEASURED RESONANT FREQUENCY^2 (LINEAR WITH STIFFNESS) WITH IMAGES SHOWING RANGE OF JOINT SIZES AND A SAMPLE FRACTURE.

fiber rods all make the relationship complex (instead of the simple relationship implied by Eqns. (1) and (3)), the trend is clear. The curve represents a range from 1.5 N to 46 N and the few points that deviated from the curve tended to perform better than expected, which could be a useful behavior for quality control. It is also noted that the single large outlier was bonded with CA that had partially set up and behaved oddly, never curing fully.

4 Conclusions and Future Work

The experiments and modeling reveal that both thermal and vibrational inspection are able to sense the presence of glue in a bond. The vibrational method provides a clearer indication of joint stiffness and likely joint quality. The measurement gives more than a hundred levels of resolution over a typical joint size range, and maintains useful sensitivity throughout that range.

The vibrational method also has some interesting logistical advantages. The energy required for the measurement comes directly from the existing drive platform making microrobot integration trivial. The signal of interest is measured acoustically making it non-contact and insensitive to alignment errors. Since the acoustic waves spread over an area, one microphone can cover multiple test sites making it unnecessary to miniaturize or move the sensor and its associated wires.

While the thermal method is limited in resolution, it provides an interesting advantage in that inspection can take place before a joint is cured making repair work potentially easier. The method may also be useful if the assembly is already a heat intensive process, mitigating many of the additional complications.

Although the vibrational inspection appears most promising, there are still many details to be addressed in future work. Reducing sensitivity to misalignment of placed rods will be important for the accuracy of the measure; perhaps examining higher modes could help as they have different sensitivities to support stiffness than the first mode. Characterizing the response for joints that are part of a multi-element truss structure with many structural modes could also prove more challenging. Using additional directional microphones and robots equipped with dampers may be helpful.

Finally, with parallel robot activity in a manufacturing setting, there will be background noise. Unidirectional microphones reduce the impact of ambient noise and a centralized computer can pause nearby noise generating tasks during measurement. Previous work [9] has also ex-

plored the option of passive diamagnetic levitation of robots to eliminate friction, which provides silent motion among other benefits.

ACKNOWLEDGMENT

We thank Sam Weiss, Barrett Heyneman, John Ulman and Steven Christensen for their many insightful conversations, as well as Tal Fix for her help with making high quality sample joints.

This material is based upon work supported by the Defense Advanced Research Projects Agency (DARPA) under Contract No. HR0011-12-C-0040.

Disclaimer: Any opinions, findings and conclusions or recommendations expressed in this material are those of the author(s) and do not necessarily reflect the views of the Defense Advanced Research Projects Agency (DARPA).

Development of the DM3 concepts and technology was supported by SRI's Engineering and Systems Division.

REFERENCES

[1] Seyfried, J., Szymanski, M., Bender, N., Estaña, R., Thiel, M., and Wörn, H., 2005. "The I-SWARM Project: Intelligent Small World Autonomous Robots for Micro-manipulation". In *Swarm Robotics*, E. ahin and W. Spears, eds., Vol. 3342 of *Lecture Notes in Computer Science*. Springer Berlin Heidelberg, pp. 70–83.

[2] Woern, H., Szymanski, M., and Seyfried, J., 2006. "The I-SWARM project". In Robot and Human Interactive Communication, 2006. ROMAN 2006. The 15th IEEE International Symposium on, pp. 492–496.

[3] Casanova, R., Dieguez, A., Sanuy, A., Arbat, A., Alonso, O., Canals, J., Puig, M., and Samitier, J., 2007. "Enabling swarm behavior in mm3-sized robots with specific designed integrated electronics". In Intelligent Robots and Systems, 2007. IROS 2007. IEEE/RSJ International Conference on, pp. 3797–3802.

[4] Donald, B. R., Levey, C. G., and Paprotny, I., 2008. "Planar Microassembly by Parallel Actuation of MEMS Microrobots". *Microelectromechanical Systems, Journal of,* ***17***(4), pp. 789–808.

[5] Frutiger, D. R., Vollmers, K., Kratochvil, B. E., and Nelson, B. J., 2010. "Small, Fast, and Under Control: Wireless Resonant Magnetic Micro-agents". *The International Journal of Robotics Research,* ***29***(5), pp. 613–636.

[6] Kernbach, S., 2011. "Swarmrobot.org - Open-hardware Microrobotic Project for Large-scale Artificial Swarms". *CoRR,* ***abs/1110.5***.

[7] Diller, E., Floyd, S., Pawashe, C., and Sitti, M., 2012. "Control of Multiple Heterogeneous Magnetic Microrobots in Two Dimensions on Nonspecialized Surfaces". *Robotics, IEEE Transactions on,* ***28***(1), pp. 172–182.

[8] Pawashe, C., Floyd, S., Diller, E., and Sitti, M., 2012. "Two-Dimensional Autonomous Microparticle Manipulation Strategies for Magnetic Microrobots in Fluidic Environments". *IEEE Transactions on Robotics,* ***28***(2), Apr., pp. 467–477.

[9] Pelrine, R., Wong-Foy, A., McCoy, B., Holeman, D., Mahoney, R., Myers, G., Herson, J., and Low, T., 2012. "Diamagnetically levitated robots: An approach to massively parallel robotic systems with unusual motion properties". In Robotics and Automation (ICRA), 2012 IEEE International Conference on, pp. 739–744.

[10] Pelrine, R., Wong-Foy, A., McCoy, B., Holeman, D., and Mahoney, R., 2011. "Micro Robot Manufacturing". In Technical Digest from Technologies for Future Micro / Nano Manufacturing, 2011. MFG 2011.

[11] Fahlbusch, S., and Fatikow, S., 1998. "Force sensing in microrobotic systems-an overview". In Electronics, Circuits and Systems, 1998 IEEE International Conference on, Vol. 3, pp. 259 –262 vol.3.

[12] Sun, Y., Nelson, B. J., Potasek, D. P., and Enikov, E., 2002. "A bulk microfabricated multi-axis capacitive cellular force sensor using transverse comb drives". *Journal of Micromechanics and Microengineering,* ***12***(6), p. 832.

[13] Arbat, A., Canals, J., Casanova, R., Dieguez, A., Brufau, J., Puig, M., and Samitier, J., 2007. "Design and control of a microcantilever tool for micro-robot contact sensing". In Circuit Theory and Design, 2007. ECCTD 2007. 18th European Conference on, pp. 100–103.

[14] Sakar, M. S., Steager, E. B., Julius, A. A., Kim, M., Kumar, V., and Pappas, G. J., 2010. "Biosensing and actuation for microbiorobots". In Robotics and Automation (ICRA), 2010 IEEE International Conference on, pp. 3141–3146.

[15] Valdastri, P., Corradi, P., Menciassi, A., Schmickl, T., Crailsheim, K., Seyfried, J., and Dario, P., 2006. "Micromanipulation, communication and swarm intelligence issues in a swarm microrobotic platform". *Robotics and Autonomous Systems,* ***54***(10), pp. 789–804.

[16] Shameli, E., Craig, D. G., and Khamesee, M. B., 2006. "Design and implementation of a magnetically suspended microrobotic pick-and-place system". *Journal of Applied Physics,* ***99***(8), Apr., pp. 08P509 –08P509–3.

[17] Eichhorn, V., Fatikow, S., Wortmann, T., Stolle, C., Edeler, C., Jasper, D., Sardan, O., Boggild, P., Boetsch, G., Canales, C., and Clavel, R., 2009. "NanoLab: A nanorobotic system for automated pick-and-place handling and characterization of CNTs". In Robotics and Automation, 2009. ICRA '09. IEEE International Conference on, pp. 1826–1831.

[18] Diller, E., Pawashe, C., Floyd, S., and Sitti, M., 2011. "Assembly and disassembly of magnetic mobile micro-robots towards deterministic 2-d reconfigurable micro-systems". *The International Journal of Robotics Research,* ***30***(14), pp. 1667–1680.

[19] Pan, J., Cheung, N. C., and Yang, J., 2003. "Structure and characteristics of closed-loop two-dimensional surface motors - a literature survey". In Power Electronics and Drive Systems, 2003. PEDS 2003. The Fifth International Conference on, Vol. 1, pp. 236 – 241 Vol.1.

[20] Teagle, P. R., 1983. "The quality control and non-destructive evaluation of composite aerospace components". *Composites,* ***14***(2), pp. 115–128.

[21] Biercuk, M., Llaguno, M., Radosavljevic, M., Hyun, J., Johnson, A., and Fischer, J., 2002. "Carbon nanotube composites for thermal management". *Applied Physics Letters,* ***80***(15), pp. 2767–2769.

[22] Meirovitch, L., 1975. *Elements of vibration analysis*. McGraw-Hill.

[23] Gibson, R. F., 2000. "Modal vibration response measurements for characterization of composite materials and structures". *Composites Science and Technology,* ***60***(15), pp. 2769–2780.

[24] Salawu, O. S., 1997. "Detection of structural damage through changes in frequency: a review". *Engineering Structures,* ***19***(9), pp. 718–723.